acoustics

MDPI

Article

On the Frequency Up-Conversion Mechanism in Metamaterials-Inspired Vibro-Impact Structures

Anuj Rekhy [1], Robert Snyder [2] and James M. Manimala [1,*]

[1] Mechanical & Aerospace Engineering; Oklahoma State University, Stillwater, OK 74078, USA; anuj.rekhy@okstate.edu

[2] Concepts 2 Systems Inc, 500, Danville, VA 24540, USA; rsnyder@concepts2systems.com

* Correspondence: james.manimala@okstate.edu

Received: 18 November 2018; Accepted: 10 February 2019; Published: 12 February 2019

Abstract: Conventional acoustic absorbers like foams, fiberglass or liners are used commonly in structures for industrial, infrastructural, automotive and aerospace applications to mitigate noise. However, these have limited effectiveness for low-frequencies (LF, <~500 Hz) due to impractically large mass or volume requirements. LF content being less evanescent is a major contributor to environmental noise pollution and induces undesirable structural responses causing diminished efficiency, comfort, payload integrity and mission capabilities. There is, therefore a need to develop lightweight, compact, structurally-integrated solutions to mitigate LF noise in several applications. Inspired by metamaterials, tuned mass-loaded membranes as vibro-impact attachments on a baseline structure are considered to investigate their performance as an LF acoustic barrier. LF incident waves are up-converted via impact to higher modes in the baseline structure which may then be effectively mitigated using conventional means. Such Metamaterials-Inspired Vibro-Impact Structures (MIVIS) could be tuned to match the dominant frequency content of LF acoustic sources. Prototype MIVIS unit cells were designed and tested to study energy transfer mechanism via impact-induced frequency up-conversion and sound transmission loss. Structural acoustic simulations were done to predict responses using models based on normal incidence transmission loss tests. Simulations were validated using experiments and utilized to optimize the energy up-conversion mechanism using parametric studies. Up to 36 dB of sound transmission loss increase is observed at the anti-resonance frequency (326 Hz) within a tunable LF bandwidth of about 300 Hz for the MIVS under white noise excitation. Whereas, it is found that under monotonic excitations, the impact-induced up-conversion redistributes the incident LF monotone to the back plate's first mode in the transmitted spectrum. This up-conversion could enable further broadband transmission loss via subsequent dissipation in conventional absorbers. Moreover, this approach while minimizing parasitic mass addition retains or could conceivably augment primary functionalities of the baseline structure. Successful transition to applications could enable new mission capabilities for aerospace and military vehicles and help create quieter built environments.

Keywords: acoustic metamaterials; vibro-impact; sound transmission loss

1. Introduction

Since the advent of the modern age and industrialization, airborne noise has gradually assumed increasing significance due to its detrimental consequences to health and safety, the lifecycle of engineered structures, mission capabilities, and the environment in general. Depending on the nature of its source, airborne noise could have a variety of spectral characteristics including broadband, narrowband or periodic dominant content. While several application-specific solutions have been successfully employed to mitigate its effects in engineered structures, practical means to eliminate

low-frequency (<~500 Hz) noise in applications where weight and volume constraints prevail have remained unaddressed. Typically, lower-frequency content is less evanescent and carries over longer aerial distances. Acoustic treatments such as mass loaded vinyl, foam [1] and fiberglass claddings and cores, layered barriers and porous materials and liners are employed effectively to mitigate high-frequency content. However, such conventional approaches tend to impose unacceptable weight and volume penalties for low-frequency noise mitigation especially in aerospace applications [2]. With increasingly stringent noise regulations being put in place to curb environmental noise pollution and mission specifications becoming more multifarious and demanding, alternate approaches to tackle low-frequency noise are of economic and operational significance.

In recent years, with current additive and hybrid manufacturing attaining critical commercial maturity, it is an opportune time to explore structural acoustic configurations that can benefit from the new materials and processes that have become available. One research area which has had exceptional progress over the past few decades and is poised to take advantage of this surge in new manufacturing techniques is that of Acoustic Metamaterials (AM). AM are manmade structural materials that derive their unique mechanical wave manipulation capabilities not just from their material constituents but more so from their engineered local configurations [3,4]. AM can exhibit frequency-dependent negative and complex effective mass density [5,6] and modulus [7–9] resulting in unusual wave phenomena [10–13]. Depending on the scale of implementation, these configurations may be deployed as microscopic inclusions in meta-composites [14] or even as macroscale endo-structures within load-bearing exo-structures [15].

The application of metamaterials-concepts to realize unprecedented physical responses has met with considerable success. Analytical, numerical and experimental investigations on negative effective mass [16–18], double negativity [19], tunable absorption in and transmission through membrane-type acoustic metamaterials [20–28], broadband noise mitigation using metamaterial panels with stacked membranes [29], impedance mismatch-driven reduction in transmitted sound energy for structures with attached gas layers [30], acoustic barriers utilizing cellular [31] and flexible [32,33] sub-structures, coupled membranes displaying monopolar and dipolar resonances [34], absorption using degenerate resonators [35], and targeted energy transfer from an acoustic medium to a nonlinear membrane [36] as well as for seismic mitigation [37] have been reported. There have been several studies ranging from tunable structural-scale AM [38,39] to active AM designs [40] that have clearly demonstrated their unique advantages. Utilizing AM to develop practical solutions for low-frequency acoustic noise mitigation is seen to be an area of emphasis. Based on these studies, it is found that there is a need for alternative, preferably passive approaches that enable low-frequency acoustic noise mitigation with little or no penalties from the perspective of practical effectiveness in applications.

In this study, a new concept of a Metamaterials-Inspired Vibro-Impact Structure (MIVIS) is investigated as a lightweight and compact barrier to understand its low-frequency up-conversion performance. MIVIS utilizes structurally integrated mass-loaded membrane attachments on a backing structure to act as tuned resonators that pick up energy from incident low-frequency sound waves and up-convert it via impacts to higher modes in the backing structure. The conceptual hypotheses and the design of the proof-of-concept test article are discussed followed by an overview of the experimental methods employed. The materials and processes involved in test article fabrication and MIVIS and baseline test cases considered are also presented. A structural acoustic simulation model was developed to predict the transmission loss spectra for the MIVIS and baseline cases. In addition to the experimental and simulated transmission loss performance vis-à-vis the baseline, the transient spectral characteristics and the low-frequency up-conversion mechanism are examined. The possibility for integration with state-of-the-art conventional acoustic treatments to deliver broadband transmission loss performance encompassing the hitherto unaddressed low-frequency regime is also demonstrated. Such MIVIS exhibit the potential to be developed into tunable yet lightweight and compact structural elements for reducing low-frequency airborne noise via up-conversion.

2. Concept and Design

Drawing inspiration from acoustic metamaterials that utilize the presence of periodic local engineered features within a host structure or material to manipulate the passage of mechanical waves through them, the MIVIS concept employs mass-loaded membranes as the vibro-impact attachment on a back structure through which low-frequency sound transmission loss is to be enhanced. The central hypothesis of this concept is that by tuning the resonance frequency of the vibro-impact membrane attachment to suit the dominant low-frequency content of the incident spectrum, sound transmission loss in this frequency range could be enhanced by up-converting the energy to higher modes of the backing structure. Further, a subsidiary hypothesis is that the up-converted energy could subsequently be dissipated using conventional acoustic absorbers such as foam in conjunction with MIVIS. For realistic sources with multiple dominant low-frequency tones, an array of tuned MIVIS unit-cells could be utilized to target a wideband frequency range.

In order to test the hypotheses and investigate the parameters that influence the vibro-impact induced energy up-conversion mechanism, a proof-of-concept test article was designed based on analytical and numerical studies. CAD drawings of the configuration and components of the MIVIS test article are shown in Figure 1, while dimensions are shown in Figure 2. The primary MIVIS test article consists of a filleted square aluminum plate back structure with a 0.508 mm (0.02″) thick ABS plastic membrane having a steel rivet impactor at its center that is held at a prescribed gap from the back structure via a set of steel spacer frames affixed to the back structure's perimeter as shown in Figure 1. Material properties for its components are listed in Table 1. These material and geometric properties result in a surface mass density of 1.76 kg/m^2 for the back plate and 0.52 kg/m^2 for the membrane. The membrane and impactor selection was based on finite element modal analysis which predicted its first symmetric mode to be 170 Hz. The proof-of-concept test article was sized to suit a custom-built normal incidence transmission loss tube [41] having a 63.5 mm × 63.5 mm (2.5″ × 2.5″) square internal cross-section as shown in Figure 3 that was used for experiments.

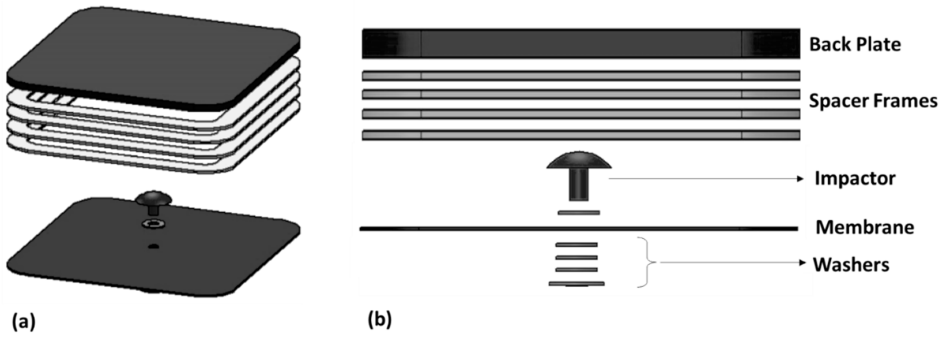

Figure 1. (**a**) Exploded and (**b**) component views of the CAD model for the MIVIS test article.

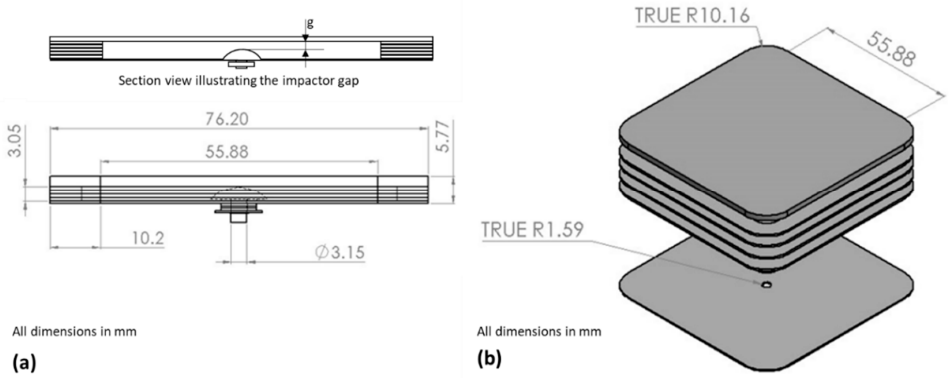

Figure 2. (**a**) Side and (**b**) isometric views of the CAD model for the MIVIS test article showing key dimensions and the gap parameter, g.

Table 1. Material properties for MIVIS components.

Component	Material	Property		
		Young's Modulus (GPa)	Mass Density (kg/m^3)	Poisson's Ratio
Back plate	Aluminum	70	2700	0.32
Spacer frames	Stainless steel	197	7900	0.28
Impactor	Steel	210	8000	0.30
Membrane	ABS plastic	2	1020	0.35

Source: Manufacturer's specifications.

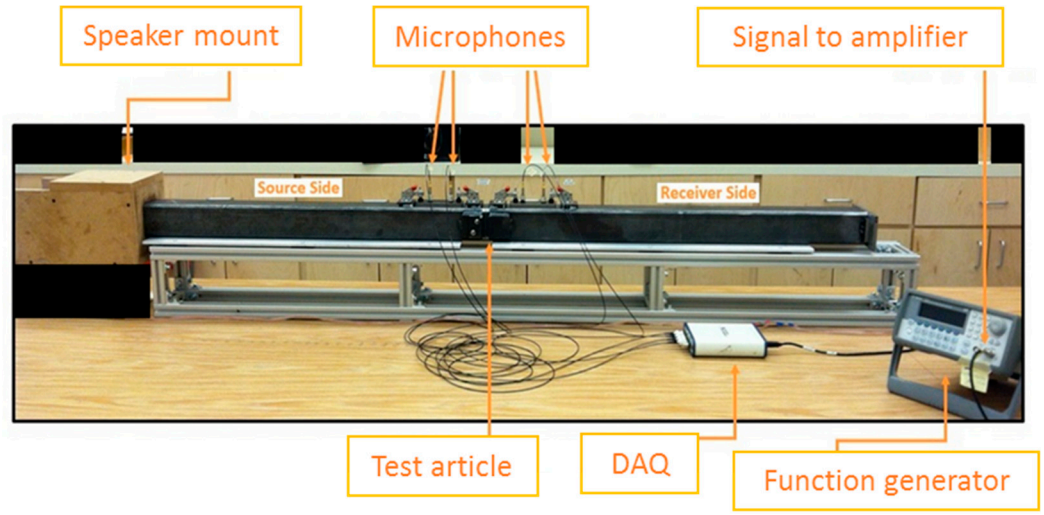

Figure 3. Normal incidence transmission loss tube.

3. Experimental Methods

3.1. Test Apparatus and Transmission Loss Measurement Procedure

The experiments in this study were conducted using a custom-built normal incidence transmission loss tube [41] shown in Figure 3 according to ASTM E2611-09 standard [42]. As per this standard, the transfer matrix method is used to reduce sound transmission loss from four microphone measurements. The setup consists of 91.4 cm (36″) long incident (source) and transmitted (receiver) side tube sections having 6.35 mm (0.25″) thick walls. The tube has a 63.5 mm × 63.5 mm (2.5″ × 2.5″) square internal cross-section. The test article is placed within an acoustically-sealed holder between the incident and transmission sides of the tube. The acoustic source is provided by a Kicker® KSC4 speaker driven by a function generator and amplifier unit. The source was set at a sound pressure level of 110 dB throughout the tests. The frequency range that is possible to be tested using this setup is 60–2600 Hz. An anechoic wedge termination is provided at the far end of the transmitted side tube to minimize reflections. Four 6.35 mm (0.25″) GRAS microphones, a pair each on the incident and transmitted sides respectively are used to make sound pressure level measurements as shown in Figure 3. These microphones are numbered 1 thru 4 sequentially from closest to the source to farthest.

From the pressure measurements made using the four microphones, amplitudes of the forward and backward components of the standing wavefield on the incident and transmitted side can be obtained.

$$A = \frac{j\left(P_1 e^{jkx_2} - P_2 e^{jkx_1}\right)}{2\sin(k(x_1 - x_2))} \tag{1}$$

$$B = \frac{j\left(P_2 e^{-jkx_1} - P_1 e^{-jkx_2}\right)}{2\sin(k(x_1 - x_2))} \tag{2}$$

$$C = \frac{j\left(P_3 e^{jkx_4} - P_4 e^{jkx_3}\right)}{2\sin(k(x_3 - x_4))} \tag{3}$$

$$D = \frac{j\left(P_4 e^{-jkx_3} - P_3 e^{-jkx_4}\right)}{2\sin(k(x_3 - x_4))} \tag{4}$$

where A and B are the amplitudes of the forward and backward components respectively of the standing wave on the incident side and similarly C and D are those on the transmitting side. j is the imaginary unit and k is the wave number. P_i are the pressures measured by the microphones and x_i are the distances to these microphones from the datum which is located on the upstream (source side) face of the test article. Once the standing wave components are obtained, the acoustic pressures and velocities on both faces of the test article are directly obtained.

$$P_s = A + B \tag{5}$$

$$P_r = Ce^{-jkd} + De^{jkd} \tag{6}$$

$$u_s = \frac{A - B}{\rho c} \tag{7}$$

$$u_r = \frac{Ce^{-jkd} - De^{jkd}}{\rho c} \tag{8}$$

where P_s and P_r are the pressures at the source and receiver side faces of the test article respectively and u_s and u_r are the particle velocities at the source and receiver side faces of the test article respectively which are separated by an axial distance of d, which is the thickness of the test article. The transfer matrix relating the pressures and velocities on the source face with those on the receiver face for a single load case is set up as follow.

$$[T] = \begin{bmatrix} T_{11} & T_{12} \\ T_{21} & T_{22} \end{bmatrix} = \begin{bmatrix} \frac{P_r u_r - P_s u_s}{P_s u_r - P_r u_s} & \frac{{P_s}^2 - {P_r}^2}{P_s u_r - P_r u_s} \\ \frac{{u_s}^2 - {u_r}^2}{P_s u_r - P_r u_s} & \frac{P_r u_r - P_s u_s}{P_s u_r - P_r u_s} \end{bmatrix} \tag{9}$$

The normal incidence sound transmission loss in dB is then given by

$$TL_{ni} = 20\log_{10}\left|\frac{T_{11} + \left(\frac{T_{12}}{\rho c}\right) + \rho c T_{21} + T_{22}}{2e^{jkd}}\right| \tag{10}$$

where ρ is the density of air and c is the speed of sound in air. The normal incidence sound transmission loss is used as a primary metric to characterize the acoustic performance of MIVIS and baseline conventional structures evaluated in this study.

3.2. Test Article Fabrication

Test articles were fabricated by assembling off-the-shelf and custom sub-components. The sub-components for the MIVIS and the assembled test article are shown in Figure 4. The ABS membrane which is fitted with the steel impactor is attached with a prescribed gap between it and the aluminum back plate using a set of chemically etched steel spacer frames that can be stacked to a precise thickness. Before being placed in the test fixture, the assembly's lateral surface is coated with an acoustic sealant to minimize the possibility of flanking paths during testing.

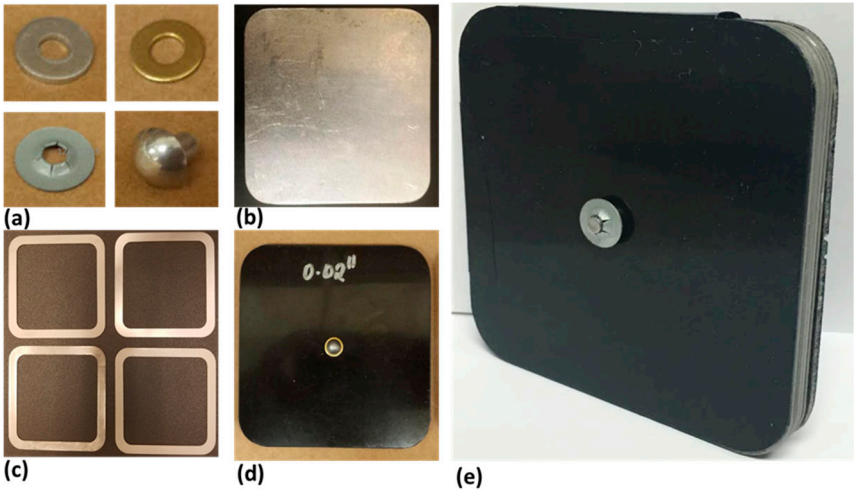

Figure 4. Components of the MIVIS test article: (**a**) washers and rivet impactor, (**b**) aluminum back plate, (**c**) steel spacer frames, (**d**) ABS membrane and (**e**) it's assembled view.

The baseline and MIVIS test articles consisting of the back plate with foam as detailed in Table 2 have the same cross-sectional dimensions as the MIVIS for evaluation in the normal incidence tube. The foam treatments were cut to size and bonded using a thin layer of adhesive to the receiver side of the back plate. Lateral surfaces are sealed for these test articles just as was done for the MIVIS.

Table 2. Experimental cases.

Case	Description	Membrane	Back Plate	Foam		Impactor Gap			Mass
		ABS Plastic, t = 0.5 mm	Aluminum, T = 0.65 mm	UL	G+	g = 0.1 mm	g = 1.0 mm	g = 1.7 mm	Approx., grams (excl. spacers)
				t_f = 25.4 mm					
1	MIVIS: small gap	✔	✔	×	×	✔	×	×	9.24
2	MIVIS: medium gap	✔	✔	×	×	×	✔	×	9.24
3	MIVIS: large gap	✔	✔	×	×	×	×	✔	9.24
4	Back plate alone	×	✔	×	×	×	×	×	7.08
5	Back plate with foam	×	✔	✔	×	×	×	×	9.64
6	Back plate with foam	×	✔	×	✔	×	×	×	9.64
7	MIVIS with foam	✔	✔	✔	×	×	×	✔	11.80

3.3. Experimental Cases

Based on preliminary trials on several combinations of membrane and back plate materials, the MIVIS test article consisting of an aluminum back plate and ABS plastic membrane was selected. Table 2 summarizes the various experimental cases considered in this study.

Three different gap settings were tested for the MIVIS. The gap between the impactor tip and the back plate was set at 0.1, 1.0 and 1.7 mm for test cases 1, 2, and 3 respectively. All other parameters were retained unaltered between these three cases. As baseline reference cases, the back plate alone (case 4) and the back plate with 25.4 mm (1-inch) thick state-of-the-art acoustic foams used in aerostructures affixed to the receiver side were also tested. Basotect® UL foam was used in case 5 and G+ foam was used in case 6. The UL foam has a bulk density of 6 kg/m^3 and the G+ foam has a bulk density of 9+/−1.5 kg/m^3 as per manufacturer's specifications. These foams have a porosity in the range of 130–200 ppi. In order to evaluate the acoustic performance of MIVIS in conjunction with foam, case 7 combines the MIVIS with the UL foam. Approximate total masses for each test case is listed in Table 2. It is worth noting that while the MIVIS test articles as listed in Table 2, weighs slightly less than the back plate with foam which is the baseline case for conventional acoustic treatment, the spacer frame's weight has not been included in these estimates since these spacers are added to alter the impactor gap in increments for experiments. In a potential version of the MIVIS for practical application, a stretched membrane having distributed impactor masses could conceivably be applied over a lightweight, lattice structure integral with the back structure. In such a version, this lightweight lattice structure would

not only provide the prescribed gap spacing for the membrane's impactors but also contribute to the stiffness and structural integrity of the back structure owing to being built into the overall design of the MIVIS composite. Both broadband white noise, as well as monotonic excitations, were used in the experiments.

4. Simulations

Structural acoustic simulations were conducted using Abaqus FEM software using a model of the normal incidence transmission loss tube test setup discussed in Section 3.1. Views of the simulation model are shown in Figure 5. The incident and transmitted side air columns in the tubes are modeled using acoustic elements with infinite impedance on the lateral surfaces to enforce the confinement offered by the tube walls. AC3D8R 8-noded acoustic brick elements are used for the air columns in the tubes, while ACIN3D8 acoustic infinite elements are used at the outboard cross-sectional face of the transmitted side tube to model the anechoic termination. The MIVIS test article is modeled using structural elements coupled to the acoustic surfaces on the incident and transmitted sides. M3D4R elements which are 4-noded membrane elements with reduced integration are used for the membrane and C3D8R elements (8-noded, reduced integration) are used for the back plate. The spacer frames are modeled as a solid rigid body. The regions along the edges of the plate clamped between the two sides of the tube in experiments were prescribed as a fixed boundary in simulations. Element sizes for individual regions were selected based on convergence and computational time studies. The source is modeled as a prescribed acoustic pressure on the outboard cross-sectional face of the incident side tube with pressure intensities and frequency content representing the experimental source. A contact surface pair is defined for the impactor and back plate surfaces that come into contact. Frictionless, hard contact interaction is assumed and the direct contact enforcement method with a fixed time incrementation scheme is employed.

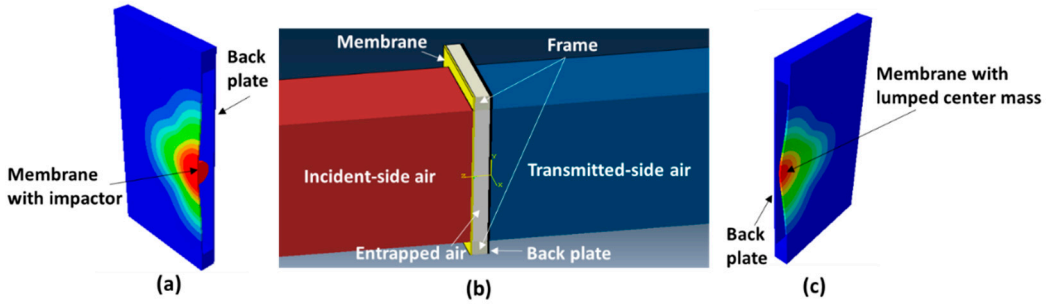

Figure 5. Views of the simulation model: (**a**) MIVIS with impactor, (**b**) transmission loss test configuration and (**c**) MIVIS with lumped center mass.

Key features that dictate the complexity and accuracy of the simulation model are the modeling approaches chosen for the entrapped air between the membrane and the back plate as well as the impactor and its contact interaction with the back plate. Several reduced order approaches were considered to evaluate their relative accuracy and efficiency to arrive at the final approach. Firstly, the effect of entrapped air and structural damping were considered for the MIVIS in the absence of contact. The impactor was modeled as a centrally-added lumped mass on the membrane. A comparison of transmission loss for some early MIVIS design cases from these simulation trials with that for the aluminum back plate which was calibrated using experiment is shown in Figure 6. As the actual modal damping in the test articles is unknown, a structural damping factor of 0.1 was used to match the transmission loss dip from the experiment for the aluminum back plate. Since the total loss in the experimental setup due to factors such as material damping, structural damping due to assembly and boundary effects, acoustic flanking paths, and dissipative mechanisms is difficult to estimate individually, the simulation model was calibrated using a static value of structural damping across the spectrum. This structural damping value, which approximates the losses in the experimental

set up is assumed to be frequency invariant for simplicity. In reality, the losses in the set up are frequency dependent and hence the simulated transmission loss could tend to vary from experiments especially near higher modes. It is noted that for the MIVIS in the absence of entrapped air in the model, a very high transmission loss is predicted due to lack of acoustic coupling between the membrane and the back plate, which is unrealistic. Therefore, it is essential to include acoustic elements with structural-acoustic coupling to the membrane and back plate in the simulation model to account for the transmission through the entrapped air. It is also noticed that while the transmission loss dips obtained for the MIVIS correlate well with the symmetric modes, the use of a frequency invariant structural damping factor would not accurately represent the actual modal damping present in the test articles and therefore the relative magnitudes of the transmission loss dips at resonance and peaks at antiresonance. Overall, diminished magnitudes and shift to higher frequencies for extrema in the transmission loss curve is noticed as the damping is increased.

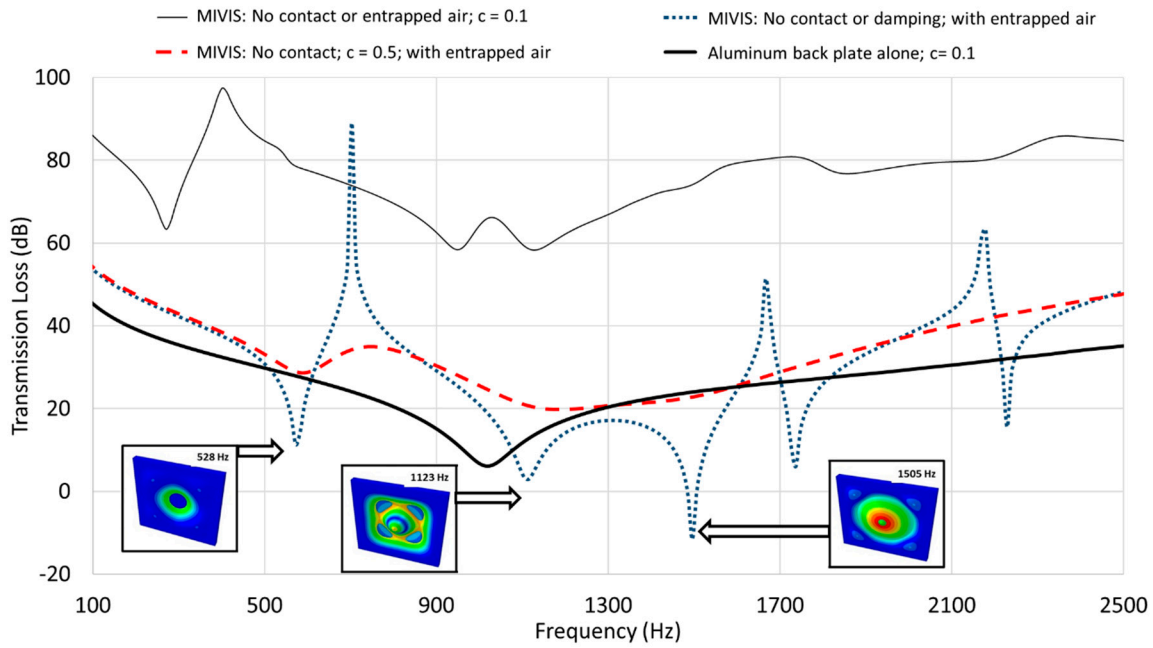

Figure 6. Simulated transmission loss curves from varying structural damping and presence of entrapped air for MIVIS without contact and for the aluminum back plate. Insets show MIVIS mode shapes corresponding to the TL dips.

For the contact simulations, the lumped center mass on the membrane for the MIVIS model was replaced by a hemispherical rigid body representative of the actual steel rivet impactor in experiments. In order to initiate and sustain contact interaction between the tip of the impactor and the back plate in the model, a circular region of the entrapped air between the tip and the back plate having a diameter half that of the impactor was retained unmeshed. The contribution of this region to transmission loss was found to be negligible in comparison to the contact-dominated response. Incident and transmitted spectra of pressure signals at the inboard microphone locations obtained from contact simulations for a tonal excitation of 564 Hz which is just above the membrane's first resonance mode (528 Hz) are shown in Figure 7. Several interesting features are noticeable. A drastic reduction in the pressure intensity between the incident and transmitted sides is seen as expected, however the generation of higher frequency content in the vicinity of the back plate's first mode at about 1100 Hz in the transmitted spectra is clearly seen at this frequency when impact-induced up-conversion is present due to the out-of-phase motion near antiresonance. This content is also seen in the incident spectra owing to the presence of the reflected component. This provides an indication that the tunable frequency range of

transmission loss increase predicted for MIVIS is accompanied by up-conversion to higher frequencies due to impact on the backing structure under monotonic excitation.

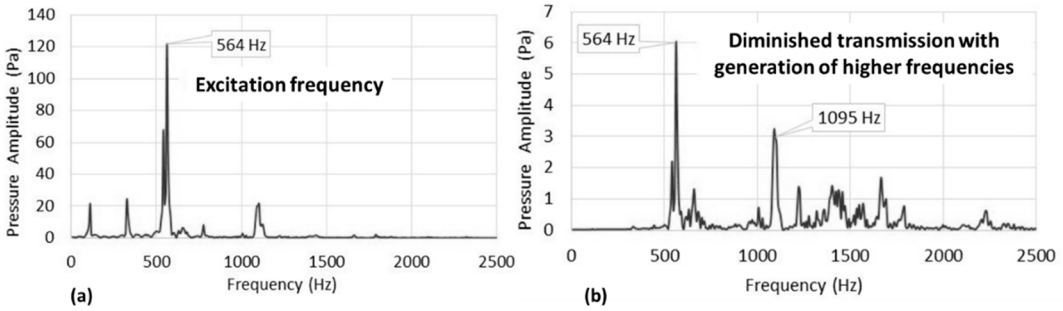

Figure 7. Simulated (**a**) incident (source-side) and (**b**) transmitted (receiver-side) pressure spectra for MIVIS with contact indicating impact-induced frequency up-conversion.

A variant of the actual MIVIS design with a membrane having a first mode below 100 Hz was also simulated to appreciate the change in up-conversion efficiency if the frequency to which the mechanism is tuned is very low. To better capture the scales involved, power spectral density comparisons for the incident and transmitted side microphone pressure signals are shown in Figure 8. It is found that the up-conversion efficiency is significantly improved to the point that the back plate's mode (1200 Hz in this case) dominates in the transmitted spectra, while the power amplitude of the excitation component is about six orders of magnitude smaller. When the separation between the membrane's tuned frequency, which is based on the excitation frequency desired to be mitigated and the back plate's first mode is large, more number of cycles of the back plate's motion is achieved between impact-induced interruptions so that a higher modal velocity is attained by the back plate leading to greater energy propagation at frequency components close to the back plate's first mode. The MIVIS and baseline experimental cases were simulated using this coupled structural-acoustic model in order to correlate the predicted mechanisms with the actual acoustic performance. Both steady state perturbation simulations under white noise excitation and transient dynamic simulations under tonal excitations were considered.

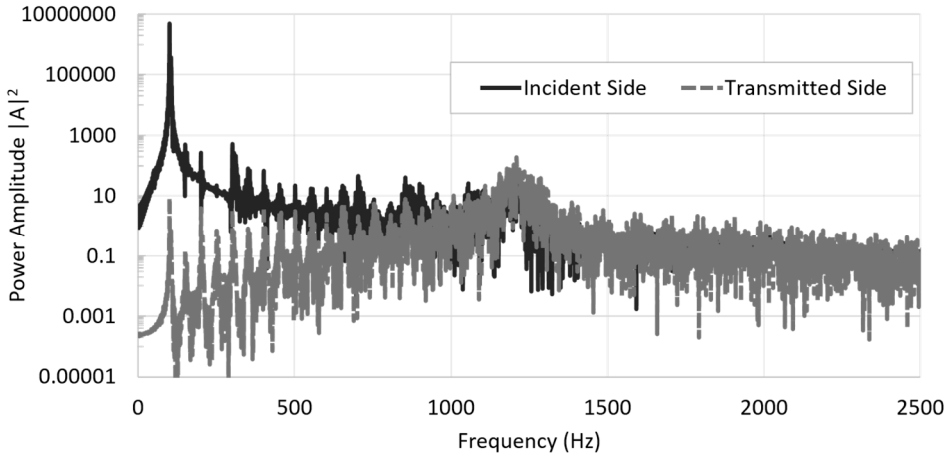

Figure 8. Simulated incident and transmitted side power spectra of pressure for MIVIS. Impact-induced up-conversion of the excitation frequency (100 Hz) to the first mode of the back plate (1200 Hz) in the transmitted spectrum is discernable.

5. Discussion of Results

Three aspects of the MIVIS test results are emphasised in the following discussion. Firstly, the transmission loss performance vis-à-vis baseline and the mechanisms involved are addressed.

Next, the transient spectral characteristics from the experiments are presented followed by the results from tests on MIVIS with foam.

5.1. Transmission Loss Performance

Comparisons of experimental and simulated transmission loss for MIVIS with those for the back plate for cases 1, 2 and 3 are shown in Figures 9–11 respectively. These cases differ in the gap setting between the impactor tip and the back plate for MIVIS. Both white noise and monotonic excitation were used in experiments. For the white noise excitation tests, case 1, which has the minimum gap (g = 0.1 mm) displays the lowest overall increase in transmission loss performance over the back plate. The bandwidth of appreciable transmission loss increase (>5 dB) is over 400 Hz in the 300 to 700 Hz region, which is the highest among the three cases with variation in the gap. A peak transmission loss increase of about 23 dB above the baseline case is obtained at 324 Hz. Case 2 with an impactor gap, g = 1.0 mm, has a bandwidth of about 300 Hz and the highest peak transmission loss increase of about 36 dB at 326 Hz. Case 3, which has the maximum impactor gap (g = 1.7 mm), has a bandwidth close to 370 Hz and a peak transmission loss increase of 31 dB at 326 Hz. The experimental and simulated transmission loss curves for the white noise case depict very close agreement, although extrema induced due to modal responses tend to have some mismatch as the exact modal damping in experiments is unknown, whereas the simulations have a frequency invariant structural damping factor of 0.1 calibrated from the baseline case. Nevertheless, the critical modal features seen in experiments in the frequency range of interest have been captured to a large extent in the simulations. The transmission loss dip locations agree very well with the first four symmetric modes predicted for the MIVIS as shown in Figure 12. Therefore, the bandwidth of transmission loss increase can be engineered to the desired frequency range by tuning these modes for the MIVIS. It is also evident from these three MIVIS cases that the up-conversion efficiency is closely linked to the gap between the impactor tip and the back plate, although bandwidth of appreciable transmission loss increase is much less affected by this. On the one hand, if the gap is inadequate (as in case 1), the membrane is unable to pick up as much energy as it could from the source due to the inability to acquire sufficient motion. On the other hand, if the gap is excessive, contact between impactor and the back plate may become impossible. It is difficult to quantitatively determine the optimal gap without more accurate knowledge of the damping in the structure and the variation in stiffness offered by the entrapped air with increase in membrane amplitude, however, case 2 with a gap, g = 1 mm, that is between the other two cases, gives the best peak transmission loss increase. This provides a qualitative indication that the optimal gap may be in the vicinity of this value for the MIVIS configuration that was tested. The transmission loss trends for the MIVIS and its equivalent double walled structure would share similarities because key structural resonances in both would be about the same. However, MIVIS incorporates the additional vibro-impact mechanism that up-converts part of the low-frequency excitation tonal energy to a higher frequency bandwidth in the vicinity of the back plate's first mode.

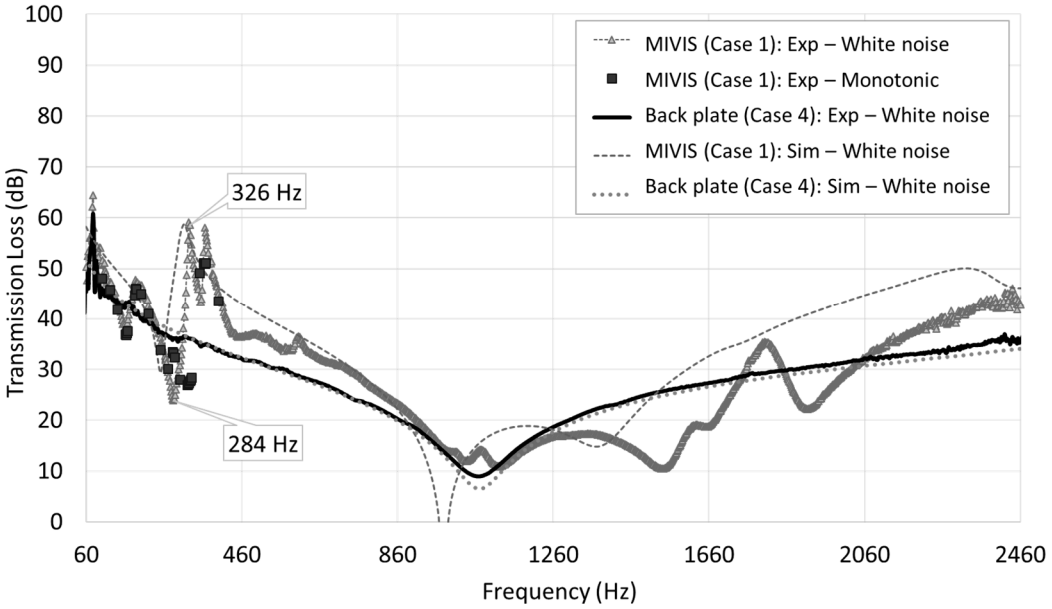

Figure 9. Comparison of simulated and experimental transmission loss for MIVIS (Case 1: g = 0.1 mm).

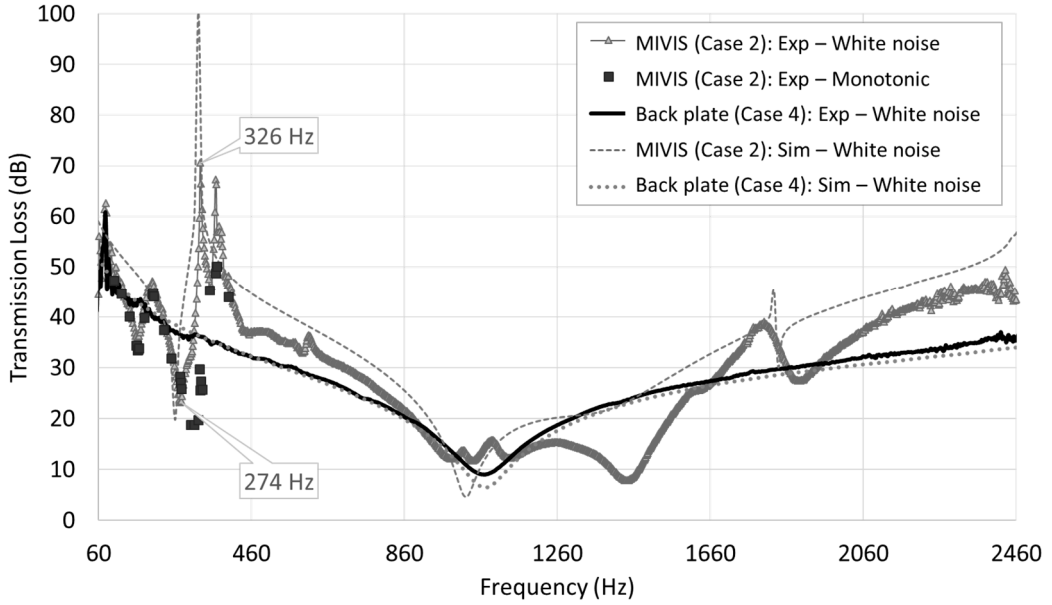

Figure 10. Comparison of simulated and experimental transmission loss for MIVIS (Case 2: g = 1 mm).

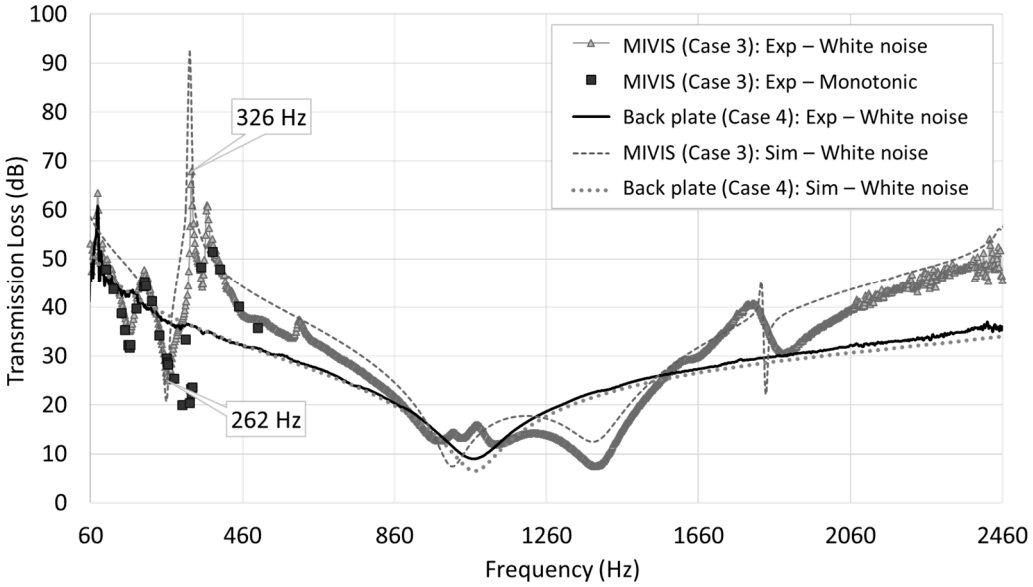

Figure 11. Comparison of simulated and experimental transmission loss for MIVIS (Case 3: g = 1.7 mm).

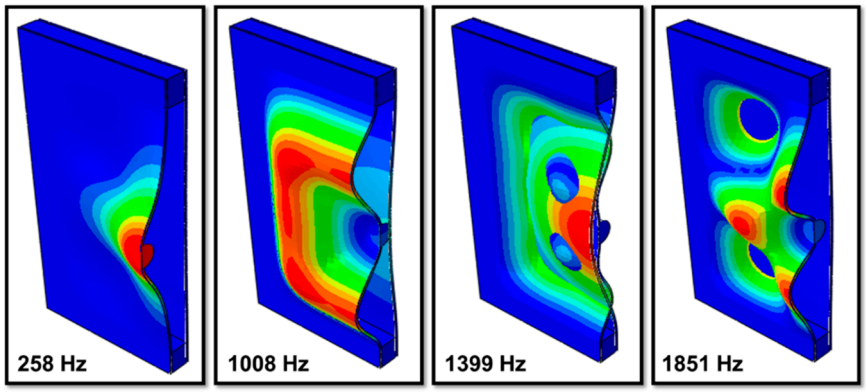

Figure 12. Simulated symmetric mode shapes for MIVIS (Case 3: g = 1.7 mm) corresponding to the dips in its transmission loss curve.

Transmission loss in the very low-frequency region from 60 Hz to ~400 Hz was also determined using monotonic excitation. Although very close agreement with white noise results is obtained from the monotonic tests in general, the phase reversal accompanying transition after the onset of resonance is observed to be delayed, while peak transmission loss increase is seen to be reduced. It is possible that the nonlinear stiffening originating from the transient build up to large amplitude motion of the membrane is manifested in the monotonic excitation test, but not in the broadband white noise test. This observation could provide a design guideline for tuning the membrane's resonance frequency to be suitable for specific bandwidths and dominant contents associated with the low-frequency source that is to be targeted.

5.2. Transient Spectral Characteristics

In order to query for the transient spectral characteristics, low, as well as high, input SPL settings were used to explore the incident and transmitted spectral evolution for the no impact, low impact and high impact behavior for various cases. These SPLs were set repeatably by changing the gain level for the amplifier to specific settings. For SPL below impact-initiation levels, the membrane deflections involved point to operation in the linear regime, whereas for the impact cases, the transition to nonlinear up-conversion should be expected. Spectrograms were generated from various test cases

to investigate the transient characteristics further. A comparison of the transmitted side spectrograms for the MIVIS (case 2) and that for the aluminum back plate alone (case 4) is shown in Figure 13. The evolution of the transmitted spectra in each case is shown as the source is operated at low power and then at high power setting. The low and high power settings for this case were chosen such that no impact occurs at low power and full impact occurs at high power for the MIVIS. For both the MIVIS and back plate cases, the monotonic incident side excitation frequency was close to 326 Hz. The amplitude of the excitation component in the incident spectra for MIVIS was noted to be nearly 600 Pa for the high power setting. Initially, when the source is operated at low power setting, the excitation component is entirely diminished in the transmitted spectra for the MIVIS, but a small component of its third harmonic is seen. For the same low power setting, a much more significant excitation component is present in the case of the back plate, while any harmonics are comparatively negligible. When the source is operated at high power setting for the MIVIS, the transmitted component of the excitation has an amplitude close to 20 Pa but is accompanied by a 10 Pa component at around 1070 Hz due to impact-induced up-conversion to the back plate's first mode. Some higher harmonic generation is also evident. Therefore, a portion of the transmitted energy is distributed to higher frequencies for MIVIS, which could be subsequently mitigated more efficiently by conventional means. In the case of the back plate, this mechanism is absent and the excitation component dominates in the transmitted spectrogram at high power.

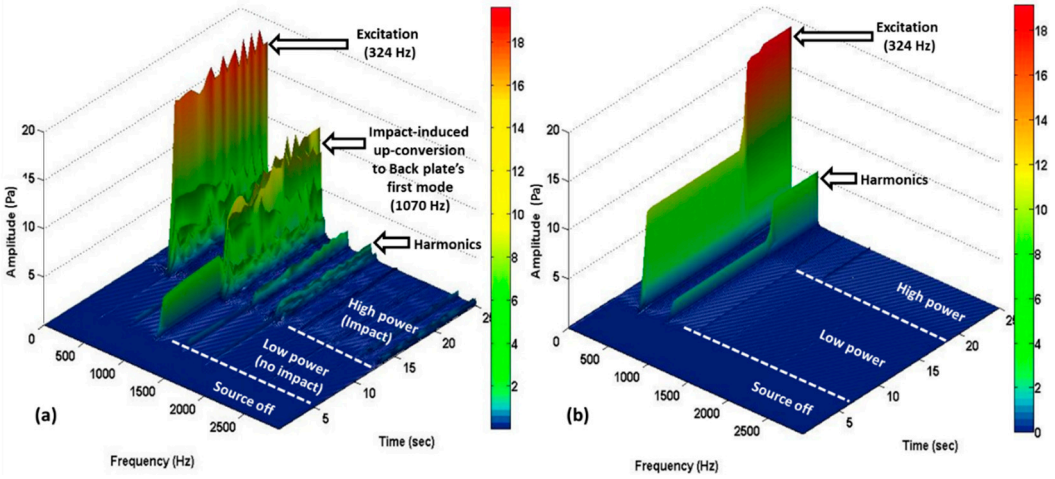

Figure 13. Transmitted side spectrograms for (**a**) MIVIS (Case 2: g = 1.0 mm) and (**b**) Aluminum back plate showing evolution through off, low power and high power settings for the source.

The comparison of the incident and transmitted side spectrograms for MIVIS (case 3) showing evolution between low and high power settings is shown in Figure 14. Here, low-intensity impact is induced at the low power setting, whereas full-fledged impact occurs at the high power setting. The incident spectrogram is clearly dominated by the excitation component at 326 Hz for both low and high power settings as is to be expected. It is interesting to note the transmitted spectral evolution when the transition occurs from low power impact to high power impact. For low power impact, only about 10% of the transmitted spectral content resides in the vicinity of the back plate's first mode. The dominant content is clearly still around the excitation component. This distribution is significantly altered under high power impact. Along with an overall decrease in the amplitude levels across the spectrum, now about 40% of the spectral content is available around the back plate's first mode. This is comparable to the excitation component in the transmitted spectrum, indicating that significant up-conversion is accomplished.

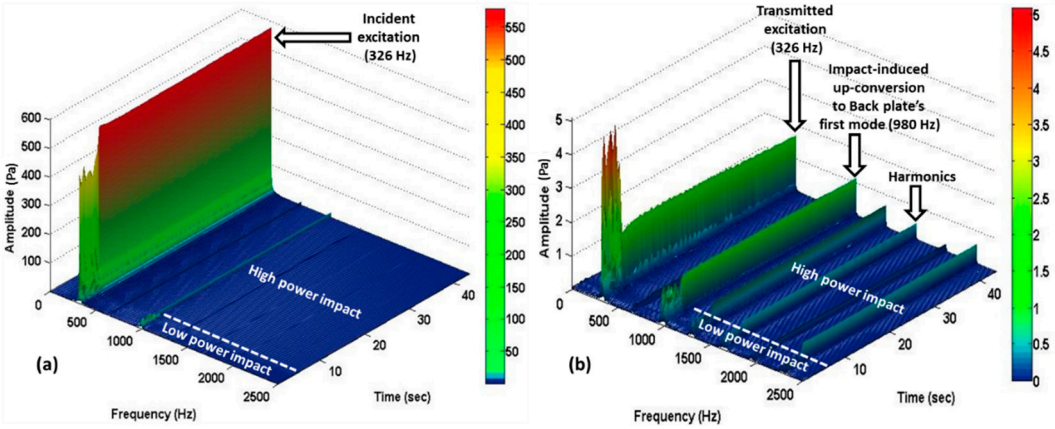

Figure 14. (**a**) Incident and (**b**) transmitted side spectrograms for MIVIS (Case 3: g = 1.7 mm) showing evolution between low and high power settings for the source.

In order to inspect the effect of the impactor gap on transient evolution of up-conversion, the transmitted spectrograms for MIVIS (case 2: g = 1.0 mm) and MIVIS (case 3: g = 0.1 mm) are compared in Figure 15. The power setting was stepped up from an initial "no contact" regime having no impact to a "contact" regime with full-fledged impact. Comparison of the relative amplitudes of the excitation and up-converted components in the transmitted spectra for both cases reveals that for the low gap (case 1), the up-converted component is restricted about 20% of the excitation component when contact is established. Case 2, which has a gap that is 10 times larger, displays an up-converted component about 40% of the excitation component, clearly illustrating the role played by the impactor gap in the efficiency of the up-conversion mechanism.

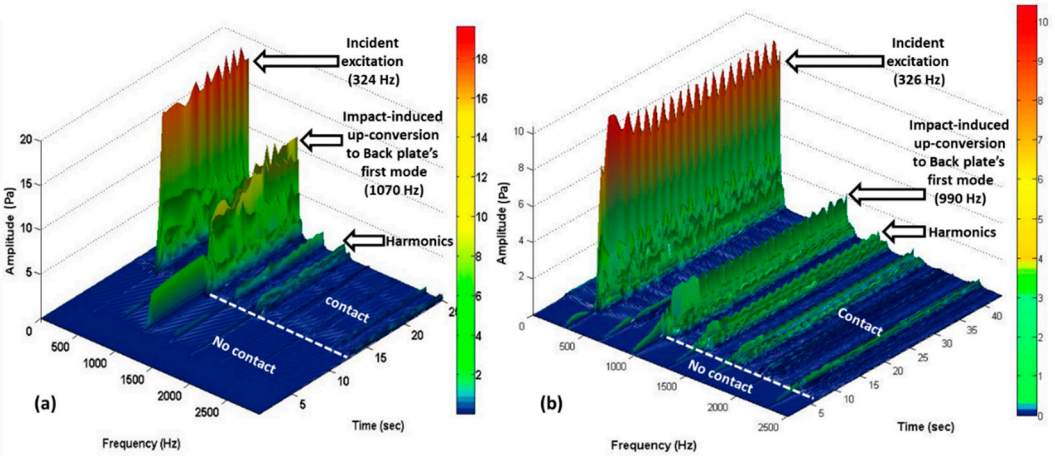

Figure 15. Transmitted side spectrogram for (**a**) MIVIS (Case 2: g = 1.0 mm) and (**b**) MIVIS (Case 1: g = 0.1 mm) showing evolution between low and high power settings for the source.

It is also interesting to note the possibility of interactive effects between the harmonics of the excitation and the back plate's first mode in the context of up-conversions in MIVIS. Since the MIVIS designs investigated in this study were tuned to up-convert a low-frequency (<~500 Hz) excitation to a sufficiently high (~>1000 Hz) value for the back plate's first mode in order to be in a frequency range where conventional absorbers start to become effective, this aspect of the excitation's harmonic being approximately close to back plate's mode was incidental rather than purposeful. However, due to the inherently nonlinear response in MIVIS, harmonic generation and interaction with the back structure's mode are a possibility worth exploring and perhaps exploiting for MIVIS design. While the interactive effects of both of these up-conversion mechanisms are not quantified, the excitation's harmonic and the

back plate's first mode are distinctly seen in the transmitted spectrogram when evolving from the low power setting to high power setting (in Figure 13 for instance). In general, it has been observed that the up-conversion efficiency is better when the separation is large between the excitation and the back plate's first mode. In such cases, it is more probable that a harmonic is closer to the back plate's mode.

5.3. MIVIS with Foam

Comparison of experimental transmission loss for MIVIS (Case 2: g = 1.0 mm) with those for aluminum back plate alone (Case 4) and for a back plate with 25.4 mm thick foam treatment (Cases 5 and 6) in the low-frequency range of interest is shown in Figure 16. While, both foams (Basotect® UL and G+ type) display a more or else uniform trend of STL increase over the back plate alone, the UL foam which has about 5–10 dB STL increase clearly outperforms the G+ foam which has only about 2–5 dB STL increase. This is expected as foams are typically better performing at higher frequencies (~1000 Hz and above.) Whereas, for the MIVIS, the presence of transmission loss peaks in the 300 to 400 Hz range resulting from the anti-resonance behavior is seen. The bandwidth of appreciable STL increase could conceivably be extended to encompass a wider low-frequency range of interest by incorporating MIVIS unit-cells with multiple tuned anti-resonances. Thus, the contrast in transmission loss performance between MIVIS and foam cases indicates the potential to combine MIVIS and foam designs to obtain interactive enhancement.

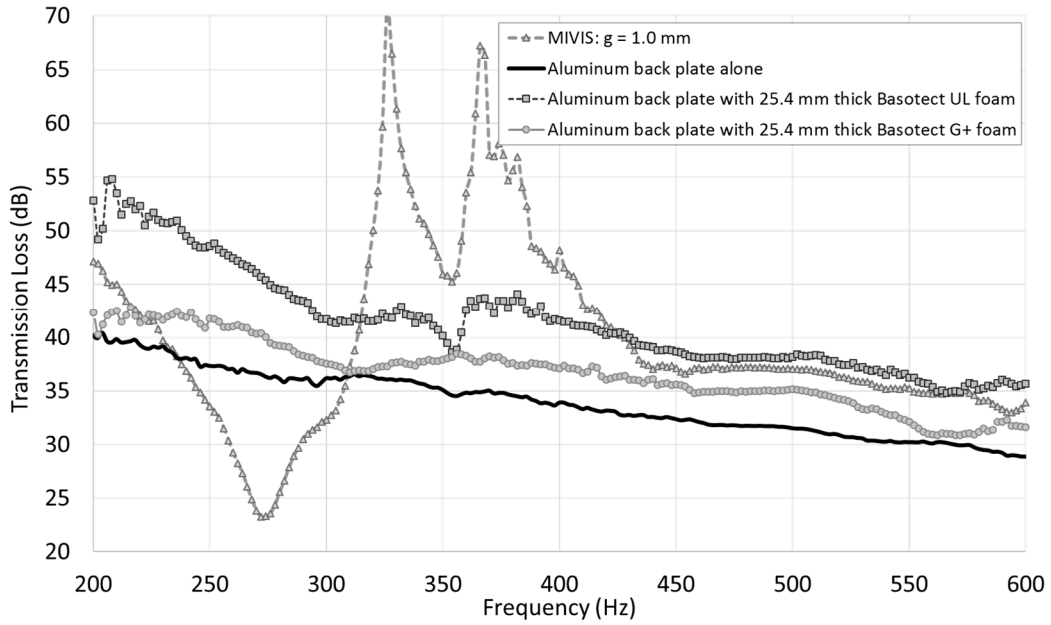

Figure 16. Comparison of experimental low-frequency transmission loss of MIVIS with those for the back plate with state-of-the-art foam treatments under white noise excitation.

The possibility of utilizing interactive mechanisms between MIVIS and foam barriers to augment STL performance is evidenced in the comparison of the incident and transmitted spectral characteristics for MIVIS alone (Case 3: g = 1.7 mm) with those for MIVIS with foam (Case 7) as shown in Figure 17. For about the same incident low-frequency spectral content centered on a tone at 326 Hz, it is observed that while low-frequency transmitted spectra is similar in magnitude and spread for both cases, the up-converted high-frequency transmitted spectral content in the vicinity of the back plate's first mode is noticeably diminished for the MIVIS with foam compared to the MIVIS alone. More than 5 dB of the decrease in the up-converted content is seen for the MIVIS with foam. It is observed that the vibro-impact induced up-conversion mechanism picks up the incident low-frequency energy of the source and makes available more of the transmitted energy at higher frequencies thereby enabling its effective mitigation using conventional lightweight absorbers such as foam. This reinforces

the subsidiary hypothesis for MIVIS that the up-conversion mechanism is amenable for coactive integration with conventional acoustic absorbers such as foam to engineer relatively lightweight structural acoustic barriers that sustain appreciable STL improvement within a broadband frequency range encompassing the hitherto unaddressed low-frequency range below ~500 Hz.

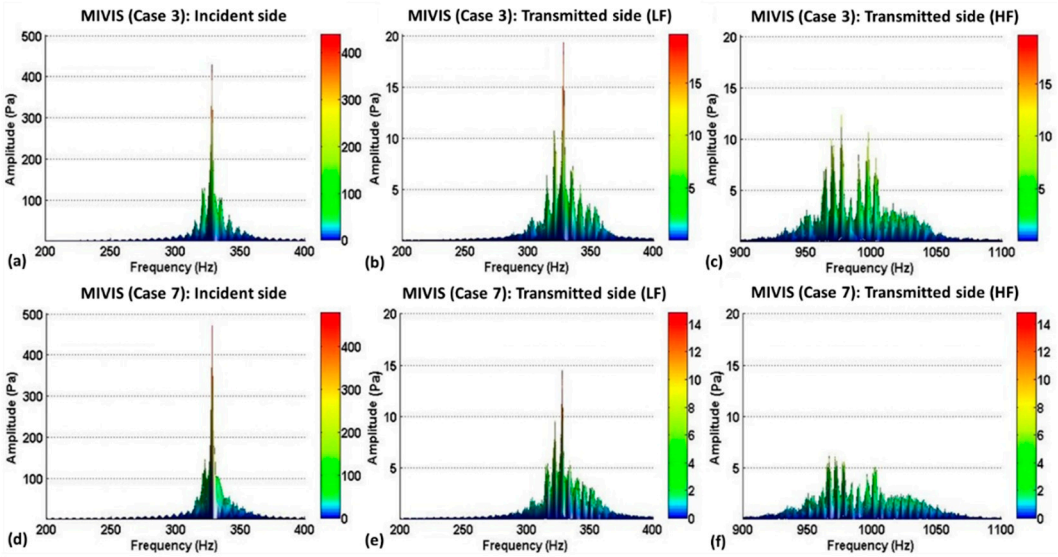

Figure 17. Comparison of the incident and transmitted side spectra for MIVIS with and without foam depicting the reduction in high-frequency content when foam is present. Panels (**a**), (**b**) and (**c**) show the incident spectrum, low-frequency and high-frequency transmitted spectra respectively for Case 3 (MIVIS: g = 1.7 mm, no foam) and panels (**d**), (**e**) and (**f**) show the incident spectrum, low-frequency and high-frequency transmitted spectra respectively for Case 7 (MIVIS: g= 1.7 mm with 25.4 mm thick Basotect UL foam).

6. Conclusions

A Metamaterials-Inspired Vibro-Impact Structure (MIVIS) concept was investigated as a lightweight and compact acoustic barrier with improved low-frequency (<~500 Hz) sound transmission loss performance. In contrast to conventional methods such as foam, fiberglass or massive treatments that are used to enhance sound transmission loss, MIVIS is compact, relatively lightweight and tunable to suit specific source characteristics. Moreover, the mechanism of frequency up-conversion via impacts to higher modes in the backing structure could be utilized to transition the incident energy to spectral bandwidths that can be effectively dissipated by conventional foams. A coupled structural-acoustic simulation model of the normal incidence transmission loss tube was used to predict and optimize the transmission loss performance of MIVIS designs. Experiments using prototype MIVIS test articles were performed to gauge their performance vis-à-vis baseline structures. Under white noise excitation, up to 36 dB of sound transmission loss increase is observed at the anti-resonance frequency (326 Hz) within a tunable LF bandwidth of about 300 Hz. The experimental and simulated transmission loss curves depict close agreement. Under monotonic excitation, an estimation of the optimal separation between the impactor tip and the back structure for efficient up-conversion was obtained. The possibility of utilizing interactive mechanisms between MIVIS and foam barriers to augment transmission loss is demonstrated. More than 5 dB of decrease in the up-converted content is seen for the MIVIS with foam. It is envisioned that the coupled structural-acoustic design approach inherent to MIVIS could be applied in specialized cases where the mitigation of particular low-frequency tones across a structural barrier become a priority. In such a design approach, the stretched membrane attachments would be affixed at separation to the base structure via a lightweight yet stiff lattice network attached to it that would create higher "local" modes in the base structure. With current additive and hybrid manufacturing attaining critical commercial maturity, successful transition to technologies that enable

new mission capabilities for aerospace and military vehicles and help create quieter built environments could become possible.

Author Contributions: Conceptualization, J.M.M.; Methodology, J.M.M.; Software, A.R. and R.S.; Validation, A.R., R.S. and J.M.M.; Formal Analysis, A.R., R.S. and J.M.M.; Investigation, A.R., R.S. and J.M.M.; Resources, R.S. and J.M.M.; Data Curation, A.R.; Writing-Original Draft Preparation, A.R. and J.M.M.; Writing-Review & Editing, J.M.M.; Visualization, A.R. and R.S.; Supervision, J.M.M.; Project Administration, R.S. and J.M.M.; Funding Acquisition, R.S. and J.M.M.

Funding: This research was supported through funding from Concepts 2 Systems Inc. for NASA SBIR Phase-I Contract No. NNX15CC41P.

Acknowledgments: Thanks are due to program monitors, Shiv Joshi (Concepts 2 Systems Inc.) and James B. Min (NASA Glenn) for their valuable inputs.

Conflicts of Interest: The authors declare no conflict of interest. No official endorsement of the contents of this paper from NASA should be inferred.

References

1. Hughes, W.O.; McNelis, A.E.; McNelis, M.E. Acoustic Test Characterization of Melamine Foam for Usage in NASA'S Payload Fairing Acoustic Attenuation Systems. 2014. Available online: https://ntrs.nasa.gov/search.jsp?R=20140008689 (accessed on 15 February 2019).
2. Munjal, M.L. *Acoustics of Ducts and Mufflers*, 2nd ed.; Wiley: Hoboken, NJ, USA, 2014.
3. Manimala, J.M. Dynamic Behavior of Acoustic Metamaterials and Metaconfigured Structures with Local Oscillators. Ph.D. Thesis, Purdue University, West Lafayette, IN, USA, 2014.
4. Lu, M.; Feng, L.; Chen, Y. Phononic crystals and acoustic metamaterials. *Mater. Today* **2009**, *12*, 34–42.
5. Huang, H.H.; Sun, C.T.; Huang, G.L. On the negative effective mass density in acoustic metamaterials. *Int. J. Eng. Sci.* **2009**, *47*, 610–617. [CrossRef]
6. Lee, S.H.; Park, C.M.; Seo, Y.M.; Wang, Z.G.; Kim, C.K. Acoustic metamaterial with negative density. *Phys. Lett. A* **2009**, *373*, 4464–4469. [CrossRef]
7. Fang, N.; Xi, D.; Xu, J.; Ambati, M.; Srituravanich, W.; Sun, C.; Zhang, X. Ultrasonic metamaterials with negative modulus. *Nat. Mater.* **2006**, *5*, 452–456. [CrossRef] [PubMed]
8. Ding, Y.; Liu, Z.; Qiu, C.; Shi, J. Metamaterial with simultaneously negative bulk modulus and mass density. *Phys. Rev. Lett.* **2007**, *99*, 093904. [CrossRef]
9. Cheng, Y.; Xu, J.Y.; Liu, X.J. One-dimensional structured ultrasonic metamaterials with simultaneously negative dynamic density and modulus. *Phys. Rev. B* **2008**, *77*, 045134. [CrossRef]
10. Huang, H.H.; Sun, C.T. Wave attenuation mechanism in an acoustic metamaterial with negative effective mass density. *New J. Phys.* **2009**, *11*, 013003. [CrossRef]
11. Yao, S.; Zhou, X.; Hu, G. Investigation of the negative-mass behaviors occurring below a cut-off frequency. *New J. Phys.* **2010**, *12*, 103025. [CrossRef]
12. Huang, H.H.; Sun, C.T. Continuum modeling of a composite material with internal resonators. *Mech. Mat.* **2012**, *46*, 1–10. [CrossRef]
13. Milton, G.W.; Willis, J.R. On modifications of Newton's second law and linear continuum elastodynamics. *Proc. R. Soc. A* **2007**, *463*, 855. [CrossRef]
14. Lakes, R.S.; Lee, T.; Bersie, A.; Wang, Y.C. Extreme damping in composite materials with negative-stiffness inclusions. *Nature* **2001**, *410*, 565. [CrossRef] [PubMed]
15. Manimala, J.M.; Huang, H.H.; Sun, C.T.; Snyder, R.; Bland, S. Dynamic load mitigation using negative effective mass structures. *Eng. Struct.* **2014**, *80*, 458. [CrossRef]
16. Yao, S.; Zhou, X.; Hu, G. Experimental study on negative effective mass in a 1D mass–spring system. *New J. Phys.* **2008**, *10*, 043020. [CrossRef]
17. Liu, Z.; Zhang, X.; Mao, Y.; Zhu, Y.Y.; Yang, Z.; Chan, C.T.; Sheng, P. Locally resonant sonic materials. *Science* **2000**, *289*, 1734. [CrossRef] [PubMed]
18. Hirsekorn, M.; Delsanto, P.P.; Batra, N.K.; Matic, P. Modelling and simulation of acoustic wave propagation in locally resonant sonic materials. *Ultrasonics* **2004**, *42*, 231–235. [CrossRef]
19. Li, J.; Chan, C.T. Double-negative acoustic metamaterial. *Phys. Rev. E* **2004**, *70*, 055602. [CrossRef]

20. Naify, C.J.; Chang, C.; McKnight, G.; Nutt, S. Transmission loss and dynamic response of membrane-type locally resonant acoustic metamaterials. *J. Appl. Phys.* **2010**, *108*, 114905. [CrossRef]
21. Naify, C.J.; Chang, C.; McKnight, G.; Scheulen, F.; Nutt, S. Membrane-type metamaterials: Transmission loss of multi-celled arrays. *J. Appl. Phys.* **2011**, *109*, 104902. [CrossRef]
22. Naify, C.J.; Chang, C.; McKnight, G.; Nutt, S. Transmission loss of membrane-type acoustic metamaterials with coaxial ring masses. *J. Appl. Phys.* **2011**, *110*, 124903. [CrossRef]
23. Naify, C.J.; Chang, C.; McKnight, G.; Nutt, S. Scaling of membrane-type locally resonant acoustic metamaterial arrays. *J. Acoust. Soc. Am.* **2012**, *132*, 2784–2792. [CrossRef] [PubMed]
24. Yang, Z.; Mei, J.; Yang, M.; Chan, N.H.; Sheng, P. Membrane-type acoustic metamaterial with negative dynamic mass. *Phys. Rev. Lett.* **2008**, *101*, 204301. [CrossRef] [PubMed]
25. Mei, J.; Ma, G.; Yang, M.; Yang, Z.; Wen, W.; Sheng, P. Dark acoustic metamaterials as super absorbers for low-frequency sound. *Nat. Commun.* **2012**, *3*, 756. [CrossRef] [PubMed]
26. Chen, Y.; Huang, G.; Zhou, X.; Hu, G.; Sun, C. Analytical coupled vibroacoustic modeling of membrane-type acoustic metamaterials: Membrane model. *J. Acoust. Soc. Am.* **2014**, *136*, 969–979. [CrossRef] [PubMed]
27. Zhang, Y.; Wen, J.; Xiao, Y.; Wen, X.; Wang, J. Theoretical investigation of the sound attenuation of membrane-type acoustic metamaterials. *Phys. Lett. A* **2012**, *376*, 1489–1494. [CrossRef]
28. Zhang, Y.; Wen, J.; Zhao, H.; Yu, D.; Cai, L.; Wen, X. Sound insulation property of membrane-type acoustic metamaterials carrying different masses at adjacent cells. *J. Appl. Phys.* **2013**, *114*, 063515. [CrossRef]
29. Yang, Z.; Dai, H.M.; Chan, N.H.; Ma, G.C.; Sheng, P. Acoustic metamaterial panels for sound attenuation in the 50–1000 Hz regime. *Appl. Phys. Lett.* **2010**, *96*, 041906. [CrossRef]
30. Naify, C.J.; Huang, C.; Sneddon, M.; Nutt, S. Transmission loss of honeycomb sandwich structures with attached gas layers. *Appl. Acoust.* **2011**, *72*, 71–77. [CrossRef]
31. Varanasi, S.; Bolton, J.S.; Siegmund, T.H.; Cipra, R.J. The low-frequency performance of metamaterial barriers based on cellular structures. *Appl. Acoust.* **2013**, *74*, 485–495. [CrossRef]
32. Ma, F.; Wu, J.; Huang, M.; Zhang, W.; Zhang, S. A purely flexible lightweight membrane-type acoustic metamaterial. *J. Phys. D* **2015**, *48*, 175105. [CrossRef]
33. Ma, G.; Yang, M.; Yang, Z.; Sheng, P. Low-frequency narrow-band acoustic filter with large orifice. *Appl. Phys. Lett.* **2013**, *103*, 011903. [CrossRef]
34. Yang, M.; Ma, G.; Yang, Z.; Sheng, P. Coupled membranes with doubly negative mass density and bulk modulus. *Phys. Rev. Lett.* **2013**, *110*, 134301. [CrossRef] [PubMed]
35. Yang, M.; Meng, C.; Fu, C.; Li, Y.; Yang, Z.; Sheng, P. Subwavelength total acoustic absorption with degenerate resonators. *Appl. Phys. Lett.* **2015**, *107*, 104104. [CrossRef]
36. Bellet, R.; Cochelin, B.; Herzog, P.; Mattei, P.O. Experimental study of targeted energy transfer from an acoustic system to a nonlinear membrane absorber. *J. Sound Vib.* **2010**, *329*, 2768–2791. [CrossRef]
37. Nucera, F.; Iacono, F.L.; McFarland, D.M.; Bergman, L.A.; Vakakis, A.F. Application of broadband nonlinear targeted energy transfers for seismic mitigation of a shear frame: Experimental results. *J. Sound Vib.* **2008**, *313*, 57–76. [CrossRef]
38. Lee, S.; Ahn, C.H.; Lee, J.W. Vibro-acoustic metamaterial for longitudinal vibration suppression in a low-frequency range. *Inter. J. Mech. Sci.* **2018**, *144*, 223–234. [CrossRef]
39. Lee, K.J.B.; Jung, M.K.; Lee, S.H. Highly tunable acoustic metamaterials based on a resonant tubular array. *Phys. Rev. B* **2012**, *86*, 184302. [CrossRef]
40. Chen, S.; Fan, Y.; Fu, Q.; Wu, H.; Jin, Y.; Zheng, J.; Zhang, F. A Review of Tunable Acoustic Metamaterials. *Appl. Sci.* **2018**, *8*, 1480. [CrossRef]
41. Callicoat, J.R. Evaluation of Composite Materials Providing Improved Acoustic Transmission Loss for UAVs. Ph.D. Thesis, Oklahoma State University, Stillwater, OK, USA, 2016.
42. ASTM: E2611-09. *Test Method for Measurement of Normal Incidence Sound Transmission of Acoustical Materials Based on the Transfer Matrix Method*; ASTM Standards: West Conshohocken, PA, USA, 2009; v04.06.